Nuclear Magnetic Resonance Analysis of Hydrothermal Reactions of Ethyl-and Octylamine in Sub- and Supercritical Water

Ken Yoshida,[*,†] *Ayato Doi,*[†] *Haruka Yoshioka,*[†,‡] *Tomohiro Hirano,*[†] *and Masaru Nakahara*[§]

[†] Department of Applied Chemistry, Graduate School of Technology, Industrial and Social Sciences, Tokushima University, 2-1, Minamijyousanjima-cho, Tokushima, 770-8506, Japan

[‡] Kurita Water Industries Ltd, 3993-15 Haijima-cho, Akishima, 196-0002, Japan

[§] Institute for Chemical Research, Gokasho, Uji, Kyoto University, 611-0011, Japan

[*] E-mail: yoshida.ken@tokushima-u.ac.jp

Abstract

Hydrothermal reactions of aliphatic amines have recently gained importance in relation to the application of amines as film-forming corrosion inhibitors for steam–water cycles. The kinetics and mechanism of the hydrothermal reactions of ethylammomiun cation ($EtAH^+$) and *n*-octylammonium cation ($OctAH^+$) were studied for comparison with the corresponding neutral amines to elucidate their reaction products and pathways at sub- and supercritical temperatures of 300–400 °C as model reactions of aliphatic ammonium cations. We analyzed the reaction of ^{13}C-^{15}N-labeled $EtAH^+$ using NMR spectroscopy and revealed that the initial hydrolysis to ethanol, known as the main path, is followed by the elimination reaction producing ethene and the disproportionation reaction giving diethylammonium cation. The $OctAH^+$ yields octene and octanol, each of which isomerizes to thermodynamically more stable species as the major products. Comparisons were made between the reactions of the neutral amines and ammonium cations to highlight their different reactivity. The hydrolysis, alkene formation, and dehydration of alcohols to alkenes were all found to be accelerated at low pH. The formation of low molecular weight organic acids such as acetic acid and formic acid was not observed. These results indicate that the corrosion protection effect of film-forming amines will be maintained under practical conditions with pH values as high as around 9 to 10, and hence side reactions involving byproducts will be suppressed.

Introduction

Insights into how strong organic bonds such as C–C, C–H, C–O, and C–N are stable or are broken in high-temperature and high-pressure water are needed from both scientific and engineering perspectives. Here, we focus on how the C–N bonds of protonated and neutral amines are cleaved and how the cleavage mechanism depends on reaction conditions such as pH and temperature. Solving this problem has become increasingly desirable in recent years due to the growing interest in alkylamines for corrosion inhibition applications in steam-water power generation cycles.[1-4] The formation of aliphatic-amine corrosion-inhibitor films is expected to ensure safe long-term operation of heat transfer from flame to hot water or steam across the metal–water interface.[5] The power generation industry today faces the challenge of balancing the introduction of massive amounts of variable renewable energy with the need to maintain a stable power supply through frequent startups and shutdowns.[6] The problem is that shutdowns accelerate corrosion due to the oxygen uptake and the localization of trace amounts of acids. To overcome this new situation, corrosion control measures need to be strengthened by a deeper understanding of the molecular sciences. In a recent study,[5] we have elucidated the film structure of alkylamines by various surface analyses; we analyzed films formed at 150 °C, a temperature sufficiently low that the effects of decomposition of amines are negligible. The reactions occurring on the water side of the water-metal interface, on the other hand, have not been fully elucidated from a physicochemical perspective. To overcome the difficulty of precisely identifying and distinguishing the structures of complex product species as a function of time, we are using a ^{13}C- and ^{15}N-labeled reactant to perform an atomic-level analysis of hydrothermal reactions with NMR for both the liquid and gas phases.

Clarification of the hydrothermal reactivity of film-forming amines (FFAs) is needed to improve the new FFA technologies and their utility. Specifically, the following aspects should be focused on. To use FFAs with less degradation and to obtain sufficient corrosion protection, the decomposition rates of FFAs and their controlling factors are to be characterized. Furthermore, it is necessary to understand what molecular species are produced in the hydrothermal reactions of FFAs and whether these product species are corrosive or not. We also need to know the extent to which the degradation of FFAs can be controlled in order to suppress the undesired effects of the decomposition products, if any, within acceptable limits. In a recent study,[7] we have investigated the decomposition reactions of ethylamine (EtA) and *n*-butylamine (BuA) as model compounds of FFAs at a supercritical temperature of 400 °C. By means of ^{1}H and ^{14}N NMR spectroscopy, we have disclosed that the initial step of the decomposition of these alkylamines is the hydrolytic cleavage of the C–N bond and that the initial products are ammonia (NH_3) accompanied by corresponding normal alcohols. A key finding is that when the amine is decomposed, NH_3 is produced in a stoichiometric amount. This result indicates that even if small amounts of corrosive organic acids are produced in side reactions, they are neutralized by the NH_3 produced in sufficient quantity. This study aims to elucidate the pathways, kinetics, and controlling factors of the reactions that occur after or in parallel with the hydrolytic deamination. The previous study[7] has suggested the presence of unidentified hydrothermal reactions of amines in addition to the hydrolytic deamination, necessitating further NMR analysis using isotope-labeled reagents. Here we show that the isotope labeling with both ^{13}C and ^{15}N isotopes is a most powerful structure-distinguishing tool

for product analysis due to its high sensitivity and scalar coupling fine structures. The target amines are expanded to include those with longer alkyl chains. The reaction of *n*-octylammonium cation ($OctAH^+$) and neutral *n*-octylamine (OctA) are explored as model substances that can more closely mimic aliphatic FFAs compared to EtA and BuA studied previously.[7] As we will show later in Results and Discussion, NMR analysis is crucial for distinguishing isomers produced by the reaction of $OctAH^+$ and OctA.

The hydrothermal decomposition of amines is a ubiquitous step in the reaction sequences of nitrogen-containing organic compounds in hot water, not only in the hydrothermal decomposition of FFAs. Ethyl- and methylamine have been reported to be intermediate products in the hydrothermal decomposition of amino acids examined at 200–450 °C,[8-10] which constitute a key step in the conversion of protein-containing biomass into valuable substances. The hydrothermal decomposition and oxidation of methylamine have been examined at 400–500 °C to understand supercritical water degradation of nitrogen-containing wastes.[11-12] Recently, Robinson et al.[13] investigated the kinetics of the hydrothermal reaction of comparatively reactive protonated benzylamines at 200–300 °C to develop a methodology for probing geological information about the inaccessibly distant past by extrapolating it to lower temperatures. Insights gained here can contribute to a deeper understanding of the hydrothermal decomposition over such a wide range of reactant species and reaction conditions. Lower amines, called alkalizing amines, are used for nuclear power applications to maintain the water in the steam–water cycles in basic conditions.[1] Studies on hydrothermal reactions of alkalizing amines have been conducted previously for

morpholine,[14-15] sarcosine,[15] 2-amino-2-methyl-1-propanol,[15] and 3-methoxypropylamine[16] mainly in the temperature range of 260–300 °C. In the field of FFA decomposition research, industrial applications have preceded fundamental academic explorations. Most conference presentations and papers have been application-oriented and focused on equipment-specific characteristics, lacking generality and universality. Regarding the decomposition temperature, for example, there has been a large discrepancy in the literature, ranging from 80 ºC to over 300 ºC.[1-2] Some literatures report the formation of a small amount of low-molecular-weight acids such as formic and acetic acids in the analysis of decomposition products in boiler water and condensate in thermal power plant applications.[17-18] Xue et al.[19] reported numerous decomposition products in the hydrothermal treatment of *N*-oleyl-1,3-propanediamine (OLDA) using a liquid chromatography coupled with a mass spectrometry, and the only product identified was 2,2′-(tridecylimino)diethanol. Most of the previous studies do not describe the reaction pathways or reaction rate equations. Thus, there is a growing need for fundamental research based on physical chemistry.

Experimental Section

Commercially available reagents were used without further purification. The reactants ^{13}C-^{15}N-labeled EtAHCl ($^{13}C2$-^{15}N; $^{13}C2$, 99%; ^{15}N, 98%) and ordinary EtAHCl (98.0%) were obtained from Cambridge Isotope Laboratories and Nacalai Tesque, respectively. The amine salt OctAHCl (98.0%) and the neutral amine OctA (98.0%) were obtained from Tokyo Chemical

Industry and Nacalai Tesque, respectively. In this study, H_2O was used as the solvent instead of D_2O to avoid the H/D exchange of hydrogens of alkyl chains, which would interfere with the analysis; the H/D exchange was reported to occur in sub- and supercritical water elsewhere.[7, 20-21] Solvent water was purified using a Milli-Q Gradient A-10 system (Merck Millipore). The solutions of the hydrochloride-salt reactants prepared at 1.0 mol kg^{-1} under ambient conditions were injected into a quartz glass tube reactor (2.0 mm i.d. and 4.0 mm o.d.). The air in the gaseous phase was exchanged with argon so that the reaction can be free from O_2 from the air, and the tube was sealed with a gas burner. When conducting the reaction of neutral OctA, OctA and H_2O were sealed in a quartz tube reactor in a phase-separated state because OctA is scarcely soluble in H_2O in ambient conditions. The amounts of OctA and H_2O were adjusted so that the molality of octylamine in the supercritical state of the solvent water is equal to 1.0 mol kg^{-1}. The density in the supercritical state was controlled by adjusting the ratio of the liquid(s) injected into the reactor under ambient conditions to its inner volume; e.g., the supercritical water density is 0.2 g cm^{-3} when the ratio is 0.2. High-temperature reactions were carried out by putting the quartz tube reactor into an electronic furnace preheated to a reaction temperature; the temperature was controlled within ±1 °C. After a reaction time, the reactor tube was taken out of the electric furnace and put into a water bath to quench the reaction. The time required for the sample to reach the reaction temperature is approximately 60 s when the reaction temperature is 400 °C. Care must be taken in evaluating the time of this temperature rise particularly when fast reactions within a time scale of 10 min or less are analyzed using the quenching method. The actual reaction time was defined by subtracting

the time of the temperature raise from the time the sample was placed in the electric furnace. The time to place the sample in the furnace was varied from 60 to 120 sec, and the dead time to start reaction was determined as the time of the temperature rise.

The reaction products were monitored using ^{1}H, ^{13}C, and ^{15}N NMR spectroscopy with JEOL ECZ400 and ECA500 spectrometers. For an NMR measurement, a quartz tube reactor was placed in a 5-mm NMR sample tube (5.0 mm o.d. and 4.2 mm i.d.). The space between the quartz tube and the NMR sample tube was filled with dimethyl sulfoxide (DMSO-d_6) (99.9% D, ISOTEC, Sigma-Aldrich) used for ^{2}H locking. A DSS-d_6 standard solution (500 mg dm^{-3} sodium 3-(trimethylsilyl)-1-propanesulfonate, FUJIFILM Wako Pure Chemicals) was used as an external reference for the integral intensity of ^{1}H NMR signals. The ^{1}H signal of water was suppressed by DANTE presaturation.[22] The ^{1}H chemical shift was externally referenced to the methyl protons of sodium 3-(trimethylsilyl)propionate-2,2,3,3-d_4 (TMSP-d_4, δ = 0.000 ppm) in aqueous solution placed in the same geometry as that of the aqueous amine solution. For quantitative analysis, the free induction decays (FIDs) for ^{1}H, ^{13}C, and ^{15}N nuclei in the liquid phase were accumulated for 16, 4, and 4 times with repetition intervals of 30, 80, and 140 s to allow the longitudinal magnetization to sufficiently relax. The gas NMR was measured for ^{1}H, ^{13}C, and ^{15}N nuclei by placing the sample tube upside down; the inner diameter of 2.0 mm is narrow enough to keep the liquid phase remaining in the upper side due to the surface tension during the measurement.[23] For the gas phase, the ^{1}H, ^{13}C, and ^{15}N signals were accumulated for 16, 128, and 128 times with repetition intervals of 30, 5, and 5 s as the longitudinal relaxation times for the ^{13}C and ^{15}N nuclei of the molecules in the gas phase are shorter. For the detailed

examination of the spectral line shape of the ^{13}C and ^{15}N signals of the products of ^{13}C-^{15}N-labeled reactants, we also performed the signal accumulation with a larger number of scans with shorter repetition intervals to achieve higher signal-to-noise ratio. For this purpose, the ^{13}C and ^{15}N signals were accumulated for 1000 times with repetition intervals of 5 and 6 sec, respectively.

In the reaction of $OctAH^+$, oil-phase products were observed. The oil-phase products were collected by opening the glass tube vessels and dissolved in $CDCl_3$ (99.80% D, 0.03% tetramethylsilane (TMS), Eurisotop). Products were collected from more than 20 reaction vessels per single NMR analysis. In this way, a concentration of 4.3–41.6 vol% of the products in chloroform solution was obtained, and a sufficient signal-to-noise ratio was achieved for the natural-abundance ^{13}C NMR analysis. As demonstrated below, the oil products were mostly octene isomers, octanol isomers, and di-*n*-octylamine. The ^{13}C signals of the products were assigned by referencing to the following authentic samples; 1-octene (FUJIFILM Wako Pure Chemicals), *trans*-2-octene (Sigma-Aldrich), 2-octene (*cis* and *trans* mixture, Tokyo Chemical Industry), *trans*-3-octene (Tokyo Chemical Industry), *cis*-4-octene (Tokyo Chemical Industry), *trans*-4-octene (Tokyo Chemical Industry), di-*n*-octylamine (96.0%, Tokyo Chemical Industry).

Results and Disucussion

Spectral Analysis of Protonated Ethylamine Reactions. Let us first examine the NMR spectra of the reaction products of protonated ethylamine ($EtAH^+$) at 300 °C on the liquid

branch of the liquid-gas coexistence curve; the density on the liquid branch and the pressure for pure water in this condition are 0.71 g cm^{-3} and 8.6 MPa, respectively.[24] In Figure 1, we show the ^{13}C spectra of the ^{13}C-^{15}N-labeled $EtAH^+$ for the sample before and after the reaction. Before the reaction (Figure 1a), only the ^{13}C signals of $EtAH^+$ and the external reference DMSO-d_6 were observed. In the spectrum for 6-h reaction in Figure 1b, four signals are newly detected and are assigned to those of ethanol (EtOH) and diethylammonium ($diEtAH^+$). It is found that EtOH is initially generated by the hydrolytic cleavage of the C–N bond, as found previously in the case of neutral EtA.[7] No other major byproducts are identified, including the formation of ketones and aldehydes; a wide range of spectra, including the low-field region, are shown in Figure S1. The ^{15}N spectrum in Figure 2 exhibits ammonium (NH_4^+) generated; the main contribution is from the hydrolysis of $EtAH^+$ and the minor one from the disproportionation of $EtAH^+$ into $diEtAH^+$.

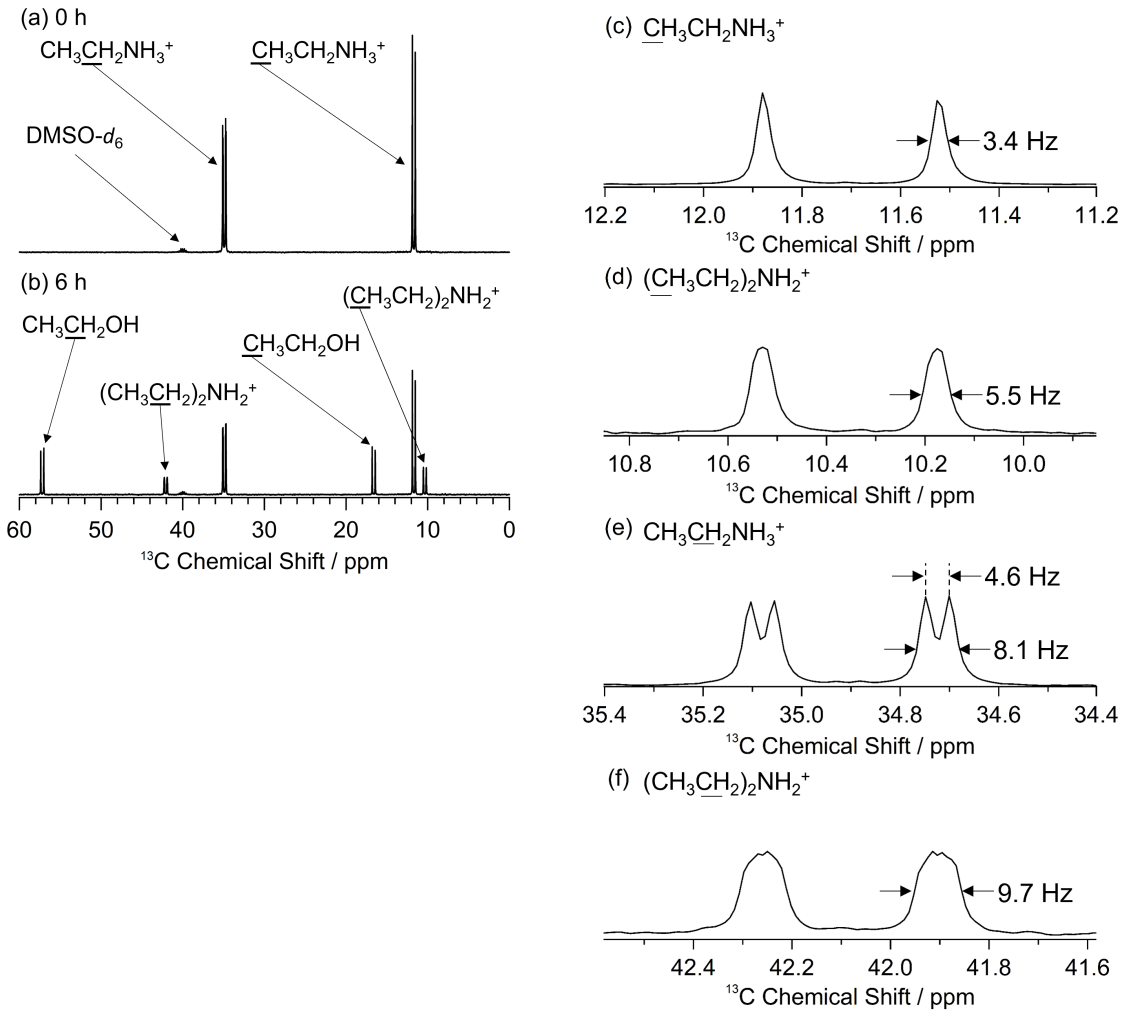

Figure 1. Liquid-phase ^{13}C NMR spectra of the aqueous solution of EtACl-$^{13}C2$-^{15}N (a) before the hydrothermal reaction (reaction time of 0 h) and (b) treated for 6 h at 300 °C on the liquid-gas coexistence curve; assignment of each ^{13}C signal is indicated by underlining the C atom in the rational formula. The enlarged views of the product signals in the panel (b) are shown in the panels (c) to (f).

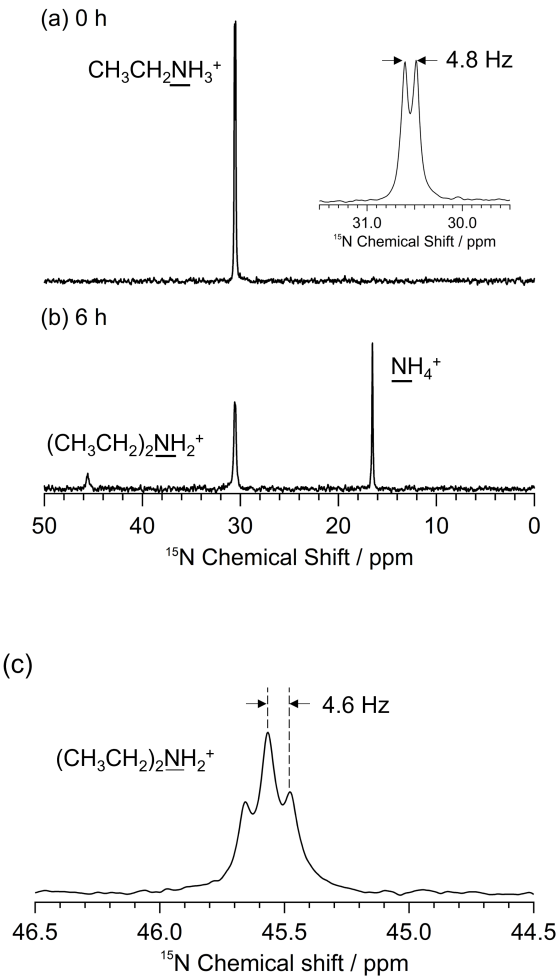

Figure 2. ^{15}N NMR spectra of the aqueous solution of EtACl (a) before the supercritical water reaction (reaction time of 0 h) and (b) after 6 h at 300 °C on the liquid-gas coexistence curve. An enlarged views of the $EtAH^+$ signal peak in the panel (a) and the $diEtAH^+$ signal in the panel (b) are shown in the inset of the panel (a) and in the panel (c), respectively. For the spectra in the panels (a) and (b), FIDs were accumulated 4 times with repetition intervals of 140 s for the quantitative analysis of signal intensities. For the high-resolution spectrum in the panel (c), FIDs were accumulated 1000 times with repetition intervals of 6 s.

It is interesting to see what products other than those described above were detected in the high-sensitivity analysis. The two new ^{13}C signals other than those of EtOH in Figure 1b are assigned to those of $diEtAH^+$ based on the couplings appearing in the spectral line shape. Detailed line shape analysis of the signals for the methyl and methylene carbons of $EtAH^+$ and $diEtAH^+$ in Figures 1c–1f allows us to reveal the presence of the secondary amine. The signals at 10.3 ppm (Figure 1d) and 42.1 ppm (Figure 1f) are assigned to the methyl and methylene carbons of $diEtAH^+$, respectively. These can be compared to the corresponding methyl and methylene carbon signals for $EtAH^+$ shown in Figures 1c and 1e. The ^{13}C signal of the methyl carbon of $diEtAH^+$ in Figure 1d is doublet due to the coupling with the adjacent methylene carbon ($^1J_{CC}$ = 35.3 Hz), common to the methyl carbon of $EtAH^+$ in Figure 1c. There exist some reasonable differences however in the spectrum caused by the difference in the bonding states between the secondary and the primary amines. The line width (full width at half-maximum height, FWHH) of each peak of the doublet for the methyl carbon of $diEtAH^+$ is 5.5 Hz, which is broader than that for $EtAH^+$ (3.4 Hz) due to the additional long-range couplings with the carbon atoms of the other ethyl group $diEtAH^+$. The ^{13}C signal of the methylene carbon of $EtAH^+$ in Figure 1e is doublet of doublets. The signal shows the larger split due to the coupling with $^{13}CH_3$, and furthermore, the top of each of those two peaks splits in two with a width of 4.8 Hz due to the coupling with ^{15}N of the amino group. The ^{13}C signal of the methylene carbon of $diEtAH^+$ in Figure 1f is also doublet of doublets. The splitting width due to the ^{13}C–^{13}C coupling is the same as that of the methyl carbon. The ^{15}N-^{13}C coupling is not clearly seen as a splitting for the methylene of $diEtAH^+$ due to the minor long-range ^{13}C–^{13}C couplings. The

FWHH of each peak is 9.7 Hz, which is much broader than that for the methyl group of $diEtAH^+$ (5.5 Hz, Figure 1d) due to the coupling with the ^{15}N nucleus of the amino group. The line width of the methylene of $diEtAH^+$ (9.7 Hz) is wider than the corresponding value of the methylene of $EtAH^+$ (8.1 Hz, Figure 1e), and this broadening by 1.6 Hz is almost the same as that of the methyl group (2.1 Hz). In the ^{15}N NMR analysis of Figure 2, the product signal at 45.6 ppm is assigned to the amino group of $diEtAH^+$ (Figure 2b). This peak is triplet (Figure 2c) due to the couplings with the two equivalent methylene carbons. The concentration values of $diEtAH^+$ determined by ^{15}N and ^{13}C agree within 10%. As the reaction time was further extended, the formation of triethylaminium ($triEtAH^+$) was also observed. The liquid-phase ^{13}C spectrum at 20 h is shown in Figure S2. Since $diEtAH^+$ is formed, it is reasonable to observe $triEtAH^+$ formed as the reaction proceeds.

Besides the saturated products discussed above, unsaturated hydrocarbon ethene (C_2H_4) has been identified. In the ^{13}C spectrum for the aqueous phase in Figure 3a, another ^{13}C peak was observed at 123.0 ppm, which was the only peak observed in the lower field region than 60 ppm; recall Figure 1b. In the gas-phase spectrum in Figure 3b, a product peak was also observed at 121.5 ppm. These peaks are assigned to C_2H_4 in a self-consistent manner as follows. The ^{13}C chemical-shift values of C_2H_4 peaks are in reasonable agreement with those reported previously for the C_2H_4 confined in a clathrate hydrate observed at 122.4–123.9 ppm, depending on the size of the cage accommodating the observed C_2H_4.[25-26] The two carbons giving the double bond peak should be equivalent because the peak is singlet. No other ^{13}C peaks were observed in the gas phase. In the ^1H spectra for the liquid phase shown in Figure

S3, we observed a pair of doublet peaks centered at 4.74 ppm, which is in satisfactory agreement with the literature value 5.28 ppm of the ^{1}H chemical shift of the proton of C_2H_4.[27] All of these liquid-phase observations lead to the consistent assignment of C_2H_4. In the gas phase, however, we did not observe any ^{1}H peak in the region of the protons of C_2H_4 probably because of the extensive broadening due to the rapid spin-rotation relaxation.[28] The concentration of C_2H_4 in the gas phase is 12.9 mmol dm^{-3} at 5-h reaction time. In a previous study on the NMR self-diffusion measurement of the low-density water at sub- and supercritical temperatures, we confirmed that the lowest limit of the water density for the ^{1}H NMR detection was about 4.1 $\times$ 10^{-3} g cm^{-3} (230 mmol dm^{-3}),[29] and below this density, the ^{1}H signal for water is too broad to use that peak for the self-diffusion measurements. In the previous report on the self-diffusion measurement of C_2H_4 by Peereboom et al.,[30] the lowest density was 6.0 $\times$ 10^{-3} g cm^{-3} (210 mmol dm^{-3}),[31] which is close to the lower limit of the water density we have previously confirmed. For these reasons, the ^{1}H signal of C_2H_4 is observed only in the aqueous phase, where the rotational motion is restricted by the neighboring solvent molecules. It is to be noted that low molecular weight organic acids such as acetic acid and formic acid were not detected.

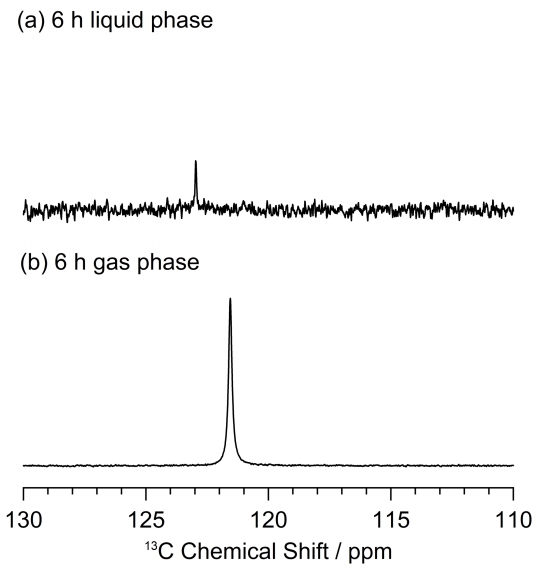

Figure 3. The carbon-carbon double-bond region of the ^{13}C NMR spectra for 1.0 mol kg^{-1} EtACl solution treated for 6 h at 300 °C on the liquid-gas coexistence curve. (a) The aqueous phase and (b) the gas phase.

Time Evolution of Protonated Ethylamine Reactions. Figure 4 shows the time evolution of the reactant and products of the hydrothermal reaction of EtACl at the reaction temperature of 300 °C and the initial concentration of 1.0 mol kg^{-1}. The reactant ammonium ion $EtAH^+$ decreases monotonically, and NH_4^+ has the highest yield among the products generated. At 6-h reaction time, the reactant decreased to 57% of its initial concentration. It is interesting to compare the hydrolysis rates of the neutral amine EtA and ammonium $EtAH^+$. To understand the hydrothermal stability, we compare the decreasing rate of $EtAH^+$ at 300 °C to that of neutral EtA previously studied at a much higher temperature of 400 °C and at 0.40 g cm^{-3}.[7] The reactant EtA decreases to ~50% of its initial amount in 6 h. This reaction time at 400 °C is comparable to that of $EtAH^+$ at 300 °C despite the large temperature difference. This

means that the reaction rate of the ammonium $EtAH^+$ is much larger than that of the neutral EtA in the same thermodynamic state. The thermal stability difference between EtA and $EtAH^+$ will be discussed in more detail below.

The carbon-containing product with the highest yield is EtOH. At 1 h, the ratio of EtOH to NH_4^+ was 0.7, and this ratio was at its maximum at this initial time in the time course. This indicates that hydrolysis of $EtAH^+$ into EtOH and NH_4^+ is dominant in the very early stage. As the reaction proceeds, the ratio of EtOH to NH_4^+ decreases, reaching 0.5 at 6 h, indicating that EtOH is further converted to other products. This ratio of EtOH to NH_3 is significantly lower for the reaction of neutral EtA measured previously.[7] In the case of neutral EtA studied at 400 °C and 0.2 g cm^{-3}, the ratio of EtOH to NH_3 is 0.27 when 90% of the reactant EtA remains, 0.15 at 32 h when 60% of EtA remains, and 0.08 at 72 h when 10% of EtA remains; the conversion of EtA at 32 h at 400 °C is close to the conversion of $EtAH^+$ at 6 h at 300 °C studied presently. The EtOH production from $EtAH^+$ is relatively larger than that from EtA because $EtAH^+$ is hydrolyzed faster, as described below. The second highest yielding product is $diEtAH^+$, which can be produced by releasing NH_4^+ from two of the parent reactant molecules. As seen in Figure 4, the production rate of $diEtAH^+$ is smaller than that of NH_4^+, but the yield of $diEtAH^+$ continues to increase monotonically, reaching 10% of the initial amount of the reactant at 6 h. This is probably because $diEtAH^+$ can also be formed by the reaction of the product EtOH with EtA.

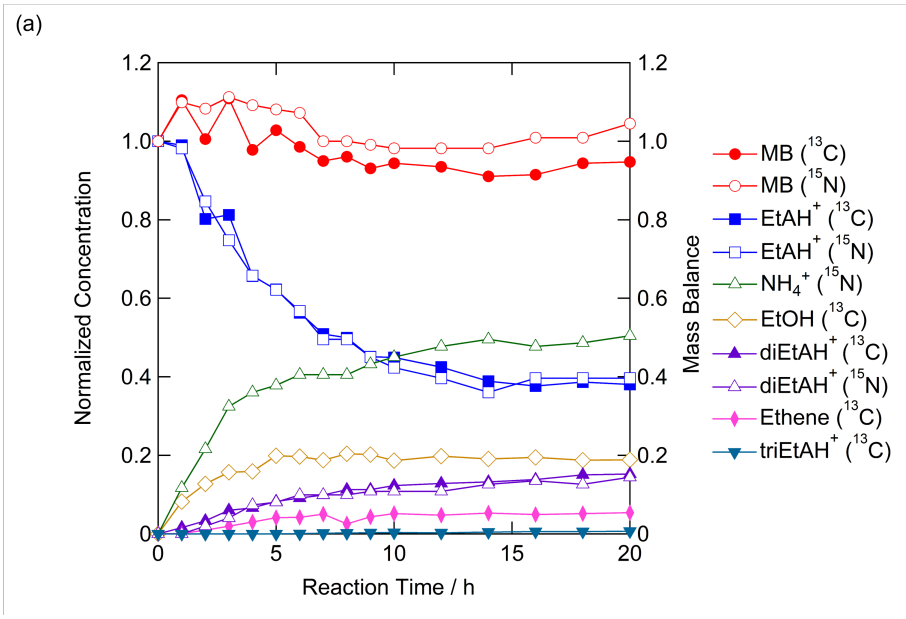
(a)
Normalized Concentration
Mass Balance
Reaction Time / h
MB (^{13}C)
MB (^{15}N)
EtAH$^+$ (^{13}C)
EtAH$^+$ (^{15}N)
NH_4^+ (^{15}N)
EtOH (^{13}C)
diEtAH$^+$ (^{13}C)
diEtAH$^+$ (^{15}N)
Ethene (^{13}C)
triEtAH$^+$ (^{13}C)

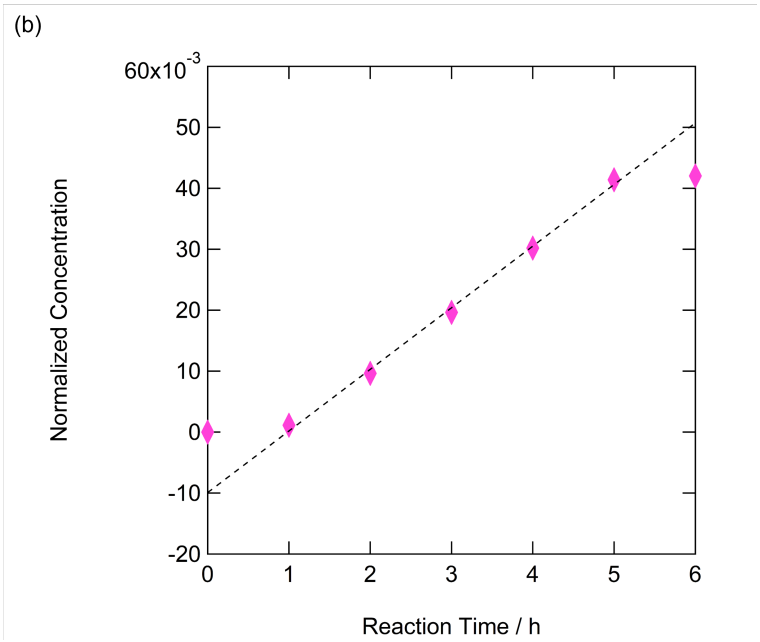
(b)
60x10^{-3}
Normalized Concentration
Reaction Time / h

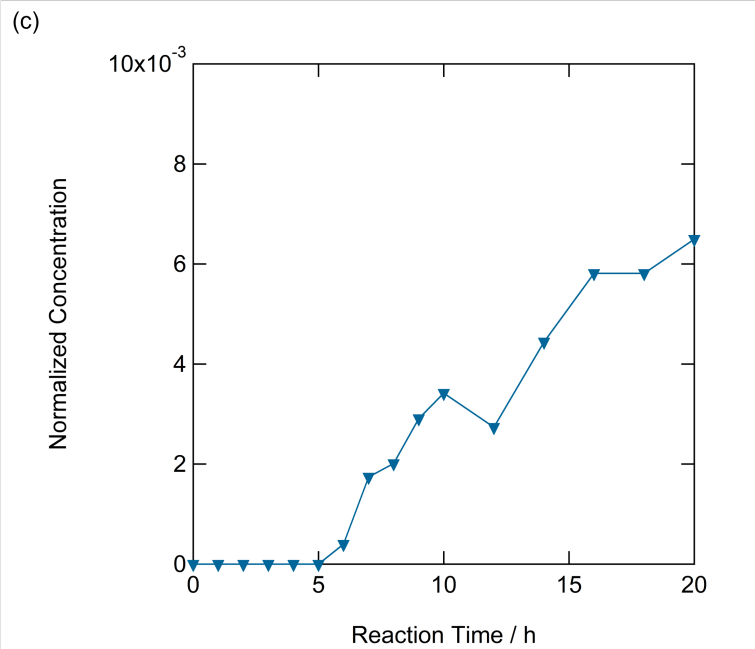

Figure 4. (a) Time evolutions of the concentrations of the reactant and products for the hydrothermal reaction of EtACl at 300 °C. The vertical axis on the left shows the normalized concentration, and that on the right shows the mass balance (MB). The normalized concentration denotes the concentration of the compound of interest divided by the initial substrate concentration. The MB denotes the ratio of the sum of the amount of nitrogen or proton atoms in the reactant and the products detected by ^{13}C or ^{15}N NMR at each reaction time divided by the amount of the corresponding nucleus of the reactant at the beginning of the reaction. (b) Enlarged view of the time evolution of the production of C_2H_4 in the initial time region. (c) Enlarged view of the time evolution of the production of triEtAH$^+$.

In the beginning of the reaction, C_2H_4 is a minor product with a yield of ~5% in 6 h. The time evolution of C_2H_4 shows that there is an induction time; an enlarged view is shown in Figure 4(b). The NMR analysis of C_2H_4 using the ^{13}C isotope is precise enough to discuss this point. The product C_2H_4 distributes dominantly in the gas phase, and its ^{13}C NMR signal can be obtained with a high signal-to-noise ratio (Figure 3b) because it can be accumulated efficiently owing to the short spin-lattice relaxation time. A linear fit of the plot in Figure 4(b)

yields an intercept with the vertical axis of -0.010 ± 0.001, which is verified to be negative; the uncertainty is shown with 95% confidence limits. The presence of the induction time indicates that C_2H_4 is a secondary hydrothermal product probably from the primary product EtOH. Direct formation of C_2H_4 by deamination of $EtAH^+$ may be possible in the bimolecular elimination (E2) mechanism, but this pathway should be minor under the hydrothermal noncatalytic conditions examined. The mass balance was determined as the sum of all products and remaining reactant described above; the results of the analysis by both ^{13}C and ^{15}N NMR are included in Figure 4. The mass balance for both ^{13}C and ^{15}N is clearly maintained within 10%. This strongly supports the reliability of the reaction pathways and the product analysis discussed above.

The concentration of the reactant $EtAH^+$ almost stops decreasing in the range of reaction times longer than 15 h. The increase of the EtOH concentration almost stops increasing after 10 h. Although the increase in $diEtAH^+$ and the associated increase in NH_4^+ continue after 10 h, the increase is clearly slower after 10 h than the increase up to 10 h. These indicate that equilibrium has been almost reached among $EtAH^+$, EtOH, $diEtAH^+$, and NH_4^+. The time evolution of $triEtAH^+$ is shown in Figure 4(c); since the concentration of $triEtAH^+$ is much lower than the other products, it is shown in a separate magnified view. The normalized concentration of $triEtAH^+$ at 20 h is 6×10^{-3}; note that the yield of the ethyl group that constitutes $triEtAH^+$ is three times larger, 2×10^{-2}, since the normalized concentrations for the products are expressed in terms of molar amount of the product species. The time evolution of

the $triEtAH^+$ concentration in Figure 4(c) shows that the formation of $triEtAH^+$ begins after 5 h. Since the formation of $triEtAH^+$ is considered to start after the formation of $diEtAH^+$, it is reasonable that the formation of $triEtAH^+$ starts later than that of other products. The generation rate of $triEtAH^+$ seems to decrease with time between 5 and 20 h; the conclusion may not be very definitive because of the small yield. Nevertheless, it seems reasonable to assume that the equilibrium amount of $triEtAH^+$ does not exceed that of $diEtAH^+$, so the order of the equilibrium amounts of the products is as follows: $EtAH^+ > diEtAH^+ \approx EtOH > triEtAH^+$. The equilibrium among the primary, secondary, and tertiary amines, and alcohols under hydrothermal conditions was recently studied by Robinson et al.[32] for benzylamine (BzA) with the corresponding molecular species. Their results showed that the abundance ratio in equilibrium was as follows: alcohol > primary amine ≈ secondary amine > tertiary amine. Although one must be careful whether the results in the presence of aromatic rings can be simply compared with those with the ethyl groups, the trends are broadly similar, at least for the equilibria among primary, secondary, and tertiary amines.

Let us discuss in more detail possible controlling factors for the yield of amines and alcohols and compare the results with those of BzA.[32] The possible controlling factors include pH, concentration, and temperature, in addition to the hydrocarbon group mentioned above. First, let us consider pH: in the case of the BzA studied by Robinson et al.,[32] they carefully minimized pH fluctuations by buffering the solution. Since the pK_a of $triBzAH^+$ is exceptionally small (pK_a = 4.9 at 25 °C), pH control by buffering is particularly effective in their case. For alkylamines, the differences in pK_a due to primary, secondary, and tertiary are

comparatively small; The pK_a values of $EtAH^+$, $diEtAH^+$, and $triEtAH^+$ at 25 °C are 10.66, 11.02, and 10.68, respectively.[33] The pK_a values of alkyl amines are available in literature[34] up to 200 °C (values above 100 °C are obtained by integrating extrapolations of dissociation enthalpies to higher temperatures), and the tendency to decrease with temperature is common to other amines including BzA as summarized in Figure S1 of ref. 32. The pK_a of ammonium is smaller than that of alkyl amines by about 1.0–1.5 from room temperature to 250 °C (Figure S1 of ref. 32). This means that the pH in our experiment fluctuates, albeit slightly, as the deamination by hydrolysis and disproportionation proceeds and approaches steady state. As for concentration, in terms of the equilibrium concentration ratio of primary to secondary amines, for example, a higher concentration has the effect of increasing the ratio of secondary amines according to Le Chatelier's principle. The concentration of the reactant primary amine in our study is 1 mol kg^{-1} and in Robinson's case 0.5 mol kg^{-1} reactant with 0.25 mol kg^{-1} NH_4Cl and 0.25 mol kg^{-1} NH_4OH for buffering. This indicates that the effect of the reactant concentration is not dominant and is overweighed by other factors. It is known that the ratio of alcohols to amines increases with increasing temperature as summarized in Fig. 1 of ref. 32. The reaction temperature for our EtA (300 °C) is higher than the temperature of BzA (250 °C) by Robinson et al.,[32] but ours yields less alcohol. This suggests that other factors, possibly the reactant molecular species, have a greater effect on the difference between the alcohol-to-amine ratios for EtA and BzA. Further discussions of these issues require higher precision values for the high-temperature pK_a and alcohol-amine equilibrium constants of each amine, which are beyond the scope of this study. In terms of the application of film-forming amines,

the conversion of the original amines to secondary and tertiary amines as well as ammonia does not interfere with keeping the system weakly basic for preventing corrosion. The formation of neutral alcohols is also not a problem. It should also be pointed out that even if carboxylic acids are formed from alcohols during longer reactions or in the presence of oxygen in the water-steam cycle, they are neutralized by more abundant ammonia or amines.

One of the most important motivations for this in-depth investigation is to elucidate the effect of protonation of the amines on the hydrothermal stability/instability. Now we consider why the protonated and neutral amines are so different. Let us compare more directly the decomposition rates of the reactants $EtAH^+$ and EtA at the same temperature of 350 °C along the liquid-gas coexistence curve. The density on the liquid branch and the pressure for pure water in this condition are 0.57 g cm^{-3} and 16.5 MPa, respectively.[24] We have chosen this thermodynamic condition so that the time scales of the decomposition of both $EtAH^+$ and EtA fall within a suitable range for monitoring the reaction. We fitted the time course of the reactant concentration to the pseudo-first-order rate equation, $d[R]/dt = -k[R]$, where [R] is the reactant concentration and k is the pseudo-first-order reaction rate coefficient. The time evolution of the reactant concentration is shown in Figure 5 and the k values determined for $EtAH^+$ and EtA at 350 °C are $(4.8 \pm 0.4) \times 10^{-4}$ s^{-1} and $(1.0 \pm 0.2) \times 10^{-5}$ s^{-1}, respectively; the rate coefficient for $EtAH^+$ is $(5 \pm 1) \times 10$ times larger than that for EtA. The greater decomposition rate coefficient of $EtAH^+$ than that of EtA corroborates the reaction mechanism we proposed previously for the hydrolytic cleavage of EtA through $EtAH^+$.[7] We previously focused on the water density effects on the hydrolysis of EtA in supercritical water and assumed the dominant

role of the protonated amino group in the hydrolysis of EtA based on the observation of the significant acceleration of the hydrolysis with increasing water density. Note that the larger the C-N bond polarity, the larger the solvation/hydration effect on transition state stability. The present results for the $EtAH^+$ reactant provide a more direct support for the proposed reaction mechanism. The density-induced shift of the equilibrium between the neutral and the protonated states to the protonated one can be an important factor in the markedly accelerated hydrolysis of neutral EtA with increasing water density.

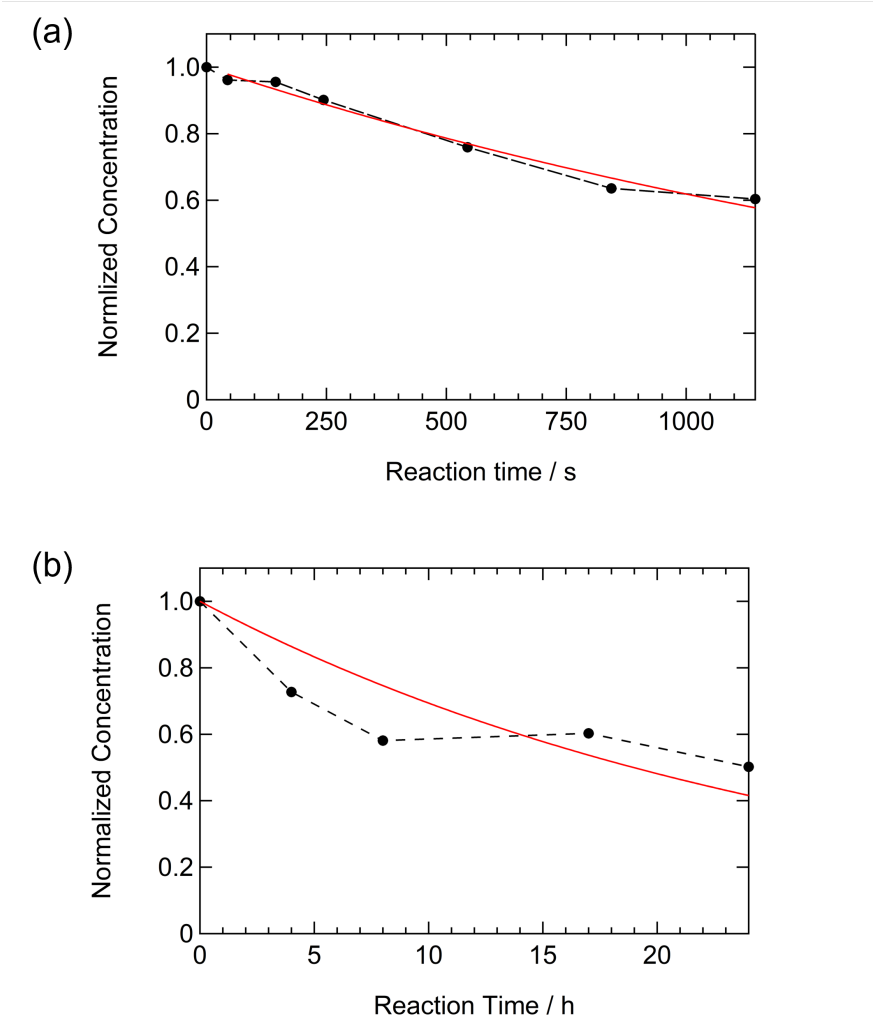

Figure 5. Time evolutions of the normalized concentrations of the reactant for the reactions of (a) EtAHCl and (b) EtA at 350 °C along the liquid branch of the liquid-gas coexistence curve.

The protonated amine $EtAH^+$ has a much larger reaction rate than the neutral one in high-temperature supercritical aqueous states. What must be paid attention to, then, is the following: since the reaction of $EtAH^+$ proceeds in a few minutes in supercritical states as shown below, the reaction time must be calibrated by excluding the time loss required for the temperature rise of the reactor as described in the Experimental Section. The time loss for the temperature increment was evaluated by extrapolating the decay curve of the $EtAH^+$ concentration to the earlier time, as shown in Figure 6. The k value at 400 °C and at 0.20 g cm^{-3} (26.4 MPa for pure water [24]) was determined to be $(1.9 \pm 0.3) \times 10^{-2}$ s^{-1}. This rate coefficient is ~3000 times larger than the previously determined EtA rate coefficient of $(6.6 \pm 0.7) \times 10^{-6}$ s^{-1}.[7] The difference between $EtAH^+$ and EtA becomes more pronounced under such low-density supercritical conditions. At lower densities with lower dielectric constants, the neutral EtA is less protonated and accordingly less reactive, which should magnify the difference in the decomposition rates of EtA and $EtAH^+$. The enhancement of the specific attractions associated with ionic species as well as polar water molecules at low densities can be another factor to accentuate the difference in the reactivity between the neutral and ionic reactants.

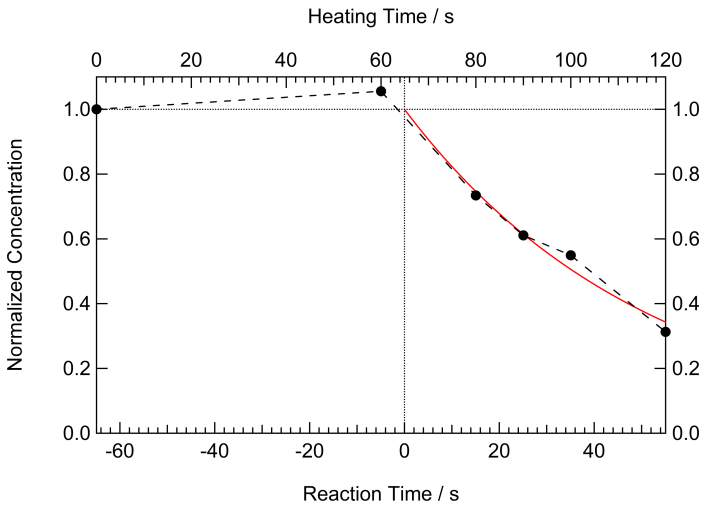

Figure 6. Time evolutions of the normalized concentrations of the reactant for the reactions of EtACl at 400 °C and at 0.20 g cm^{-3}. The decrease curve as a function of heating time was extrapolated to the short side time, and the time when the curve intersected the horizontal line indicating the initial concentration was determined as the heating time. The heating time to reach the reaction temperature of 400 °C was thus determined to be 65 s.

We propose the overall reaction scheme for $EtAH^+$ as illustrated in Figure 7. The possible reaction mechanisms are summarized in Figure 8. Figure 7 contains all possible pathways, including those with small contributions; the contribution weight of each path is discussed below. As mentioned above, the initial reaction is dominated by the deamination of $EtAH^+$ that produces EtOH and NH_4^+ by hydrolysis. This reaction can occur through the unimolecular nucleophilic substitution (S_N1, Figure 8a) and bimolecular nucleophilic substitution (S_N2, Figure 8b). The S_N1 reaction is an elimination/addition reaction via a carbocation intermediate. The addition of water can also occur directly without going through the carbocation intermediate via the S_N2 reaction. The contribution of these two mechanisms has been previously explored by Robinson et al.[13, 35] for the more reactive reactant benzylammonium ($BzAH^+$) in hot water

at 200–300 °C from the viewpoint of the effects of aromatic functional groups. They reported that at 250 °C the contribution of S_N1 and S_N2 mechanisms are comparable, that at the lower temperatures the S_N2 mechanism contributes more, and that at the higher temperatures the S_N1 mechanism, whose transition state is entropically favorable, becomes more dominant. In contrast to $BzAH^+$, $EtAH^+$ requires higher temperatures, 300–400 °C, for the hydrolysis. This indicates that both the carbocation intermediate via S_N1 and the transition state via S_N2 for the reaction of $EtAH^+$ are less stable than those for the $BzAH^+$ due to the lack of the resonance stabilization effect. Furthermore, it is assumed that $EtAH^+$ favors S_N2 when compared with $BzAH^+$ at the same temperature due to the lack of resonance stabilization effects on the carbocation. Meanwhile, the higher reaction temperature of $EtAH^+$ has the effect to increase the contribution of S_N1. To further investigate this point, experimental studies of substituent effects and kinetics, along with quantum calculations, will be needed.

Regarding the C_2H_4 formation from $EtAH^+$, there are two possible mechanisms by which C_2H_4 is formed directly from $EtAH^+$: one is the unimolecular elimination (E1) via carbocation (Figure 8c) and the other is the E2, which directly results in the formation of C_2H_4 (Figure 8d). Additionally, there are two other pathways for the C_2H_4 formation, E1 and E2 from ethanol, as shown in Figures 8e and 8f, respectively. The observed delay for the C_2H_4 formation suggests that the contribution of the E2 from EtOH is dominant in the formation of C_2H_4 and the direct paths from $EtAH^+$ are not major.

The observed delay in the C_2H_4 formation can be discussed in terms of the reaction pathway as follows. Of the two mechanisms E1 and E2 in the pathway from EtOH to C_2H_4, the

E2 mechanism, which does not go through the carbocation, can be dominant. If the primary carbocation were considerably stable in the pathway, the $EtAH^+$ to C_2H_4 pathway would also be open. This contradicts the observation that C_2H_4 is not formed in the beginning. Therefore, the barrier to the formation of the carbocation should be high enough to satisfy this condition. In this respect, the interpretation that E2 from EtOH to C_2H_4 is the dominant C_2H_4-forming pathway agrees with what was observed. In the previous literature, the main reaction mechanism was considered to be E2, based on the result that the acid concentration affects the reaction rate for 1-propanol[36] and ethanol.[37]

It is important to note that under weakly acidic conditions, as in the present experiment with hydrochloride salt as the reactant, it cannot be excluded that carbocation is more likely to be formed from EtOH than from $EtAH^+$. Although it is practically impossible to estimate the population of the protonated state $EtOH_2^+$, there should be a tendency for the protonated populations to be higher under acidic conditions. Given this, it is reasonable to assume that not only E2 but also E1 contributes to some extent to the reaction of EtOH to C_2H_4. In the previous literature, it has been argued that the possibility of E1 is ruled out by the fact that the linear dependence on acid concentration has no significant positive intercept and passes almost through the origin.[36] However, it may not be easy to distinguish the difference between E1 and E2 in sub- and supercritical water in terms of whether the elimination of H_3O^+ is stepwise or simultaneous (Figures 8c and 8d); at such high temperatures the increased molecular motion of solute and solvent significantly accelerates hydration and dehydration. Therefore, whether the two mechanisms can be clearly distinguished as stepwise or simultaneous may be a matter

of renewed debate. A deeper investigation of the reaction dynamics by computational chemistry is desirable with an explicit treatment of the solvent to unravel this issue.

For the formation of $diEtAH^+$ from $EtAH^+$, there are two possible mechanisms: S_N1 (Figure 8g), in which EtA in equilibrium with $EtAH^+$ binds to the carbocation, and S_N2, in which $EtAH^+$ and EtA couple (Figure 8h). The contribution of these two mechanisms is parallel to the involvement of the carbocation in the formation of EtOH from $EtAH^+$. The synthesis of a secondary amine with ethyl halide as the reactant is described in a textbook[38] to proceed via the S_N2 mechanism; though the temperature is not explicitly specified, it should be assumed to be near room temperature. Similar to the formation of C_2H_4 that is likely to occur in the E2 mechanism, the formation of $diEtAH^+$ can also occur in the S_N2 mechanism. At higher temperatures, S_N1 can also contribute to some extent, in contrast to room temperature. Another possible pathway for the formation of $diEtAH^+$ is the binding of EtOH to EtA by the S_N1 and S_N2 mechanisms (Figures 8i and 8j). These mechanisms require EtOH as a reactant and may be effective with longer reaction times compared to the binding of $EtAH^+$ to EtA in Figures 8g and 8h. The discussions regarding the S_N1 and S_N2 contributions may be similar to those regarding the reaction of $EtAH^+$ with EtA. Furthermore, as with the discussion on the E1/E2 mechanism of EtOH to C_2H_4 (Figures 8c and 8d), the possibility of a significant contribution of $EtOH_2^+$ may be worth considering. This is because, although the equilibrium concentration of $EtOH_2^+$ is unknown, once $EtOH_2^+$ is formed, H_2O is a good leaving group.

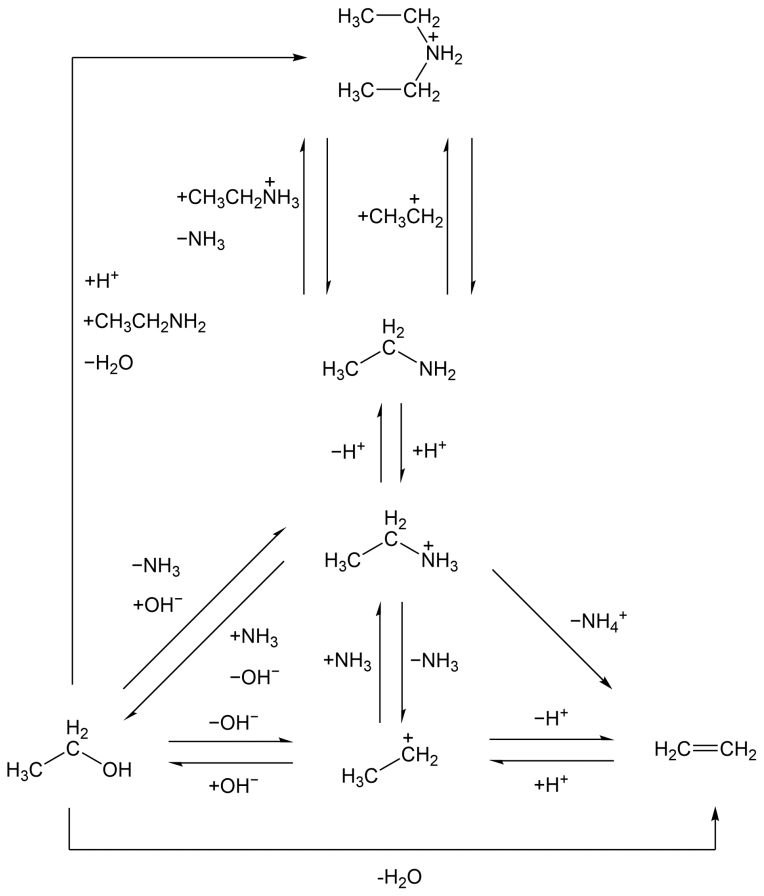

Figure 7. Reaction scheme of $EtAH^+$ in sub- and supercritical water.

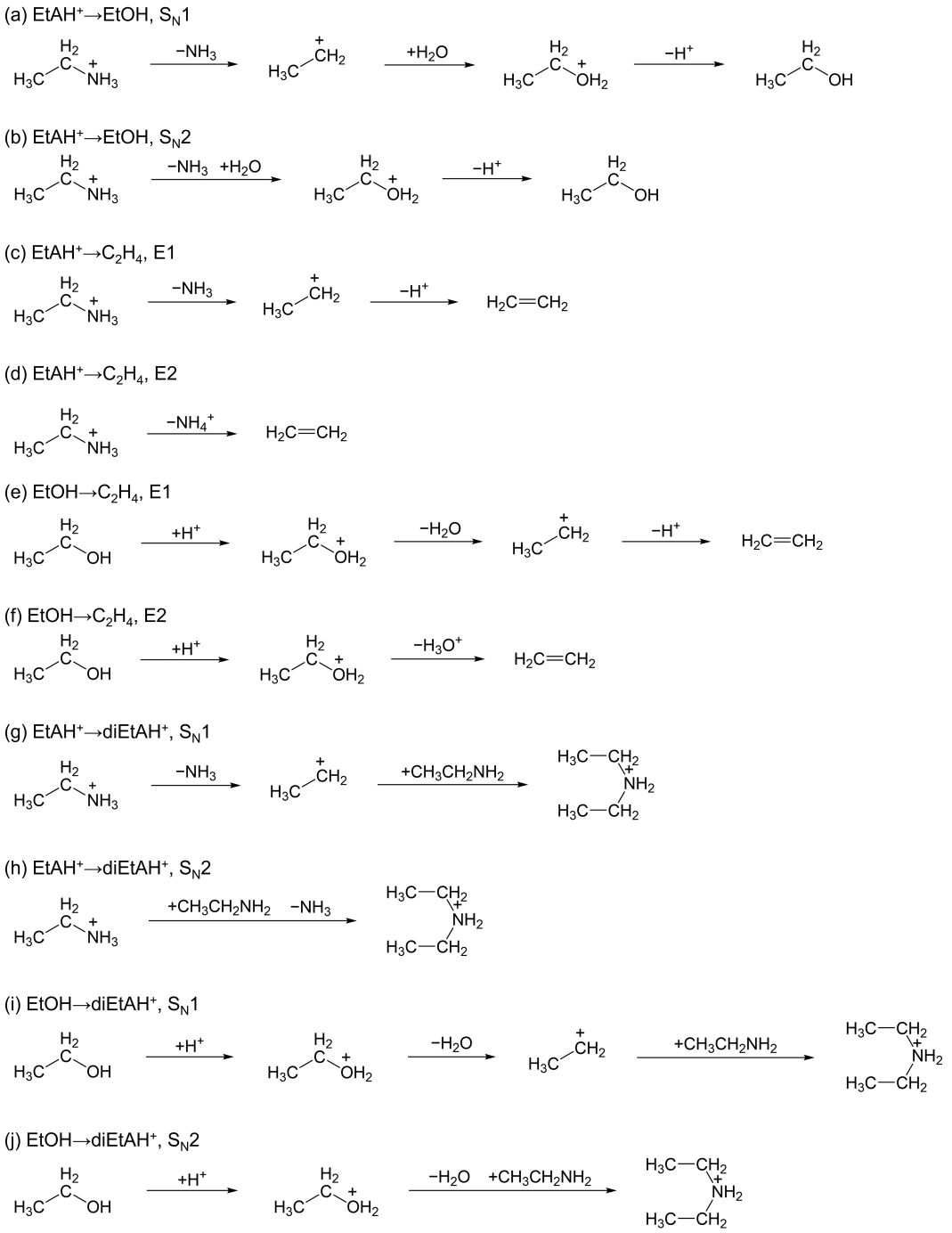

Figure 8. Reaction mechanisms for the substitution and elimination of $EtAH^+$ in sub- and supercritical water.

Reaction Products of Protonated Octylamine. The *n*-octylamine OctA is closer than EtA to the aliphatic amines utilized as practical FFAs. First, we highlight the reaction of OctAHCl whose reactions are so rapid that most product species are more detectable within the observed reaction time. The hydrothermal reaction of 1.0-mol kg^{-1} non-labeled OctAHCl was explored for 10 min at 400 °C with 0.2 g cm^{-3}. After the hydrothermal reaction was quenched, an oil phase floating on the aqueous phase was found in the reaction vessel. The volume of the produced oil phase was 17% of the volume of the aqueous phase before the reaction at room temperature. The oil phase amounts to 95% yield of the reactant. As discussed below, the NMR analysis has revealed that the oil is predominantly composed of octene isomers with a small amount of octanol isomers. The elemental analysis of the oil products showed that the mass fractions of hydrogen and carbon are 13.0% and 84.5%, respectively, and the nitrogen content was below the detection limit. The mass ratio of hydrogen to carbon is 0.154, a value slightly smaller than that of the monounsaturated linear hydrocarbon (0.167) and well below that of the saturated one (0.188). With the formation of the oil phase, the aqueous phase volume decreased to 83% of the initial volume. The amount of the remaining reactant $OctAH^+$ after the 10-min reaction was only 1.3% of the initial value, all of which was observed in the aqueous phase. Essentially no products were detected in the gas phase.

The reaction products in the oil phase were collected as described in the experimental section and analyzed using ^{13}C NMR. Figure 9 shows the ^{13}C NMR spectrum of the oil products dissolved in $CDCl_3$. The spectrum is characterized by intense signals around 110–140 ppm, which corresponds to the frequency region of carbon atoms forming double bonds. The signals with high intensities in the double-bond region are assigned to the isomers of octene (C_8H_{16}); see panels (b) and (c) of Figure 9. To identify the position of the double bond, we compared the chemical shift values with those of authentic standards for 1-C_8H_{16}, 2-C_8H_{16} (*cis* and *trans* mixture), *trans*-2-C_8H_{16}, *trans*-3-C_8H_{16}, *trans*-4-C_8H_{16}, *cis*-4-C_8H_{16}; the peaks for *cis*-3-C_8H_{16} were compared with the literature values.[39] The total yield of octene isomers was 90%. The other fractions in the oil phase were octanol isomers; the ^{13}C NMR signals of octanol isomers are shown in Figure 9d and the yields of 1-, 2-, 3-, 4-OctOH are 4.5%, 0.5%, 0.3%, and 0.2%, respectively. The equilibrium amounts of alkyl alcohols and alkenes with carbon numbers from 2 to 8 are summarized in Figure 9 of the review by Shock et al.[40] as a function of temperature in the range of 0–350 °C. The molecular species with higher equilibrium abundances are found to shift from alcohols to alkenes with increasing temperature, which is consistent with the present result showing dominant alkene yields at 400 °C. The product 1-C_8H_{16} can be formed by the following two pathways: one is the direct formation by elimination of NH_4^+ from $OctAH^+$ and the other is the dehydration of 1-OctOH into 1-C_8H_{16}. The other C_8H_{16} isomers are considered to be produced by the subsequent rapid conversions between linear octene isomers under hydrothermal conditions. The reaction scheme will be discussed

in more detail later. Almost no polymerization occurs because no broadened signal assignable to the polymer main chain is observed in the ^{13}C spectrum (Figure 9a).

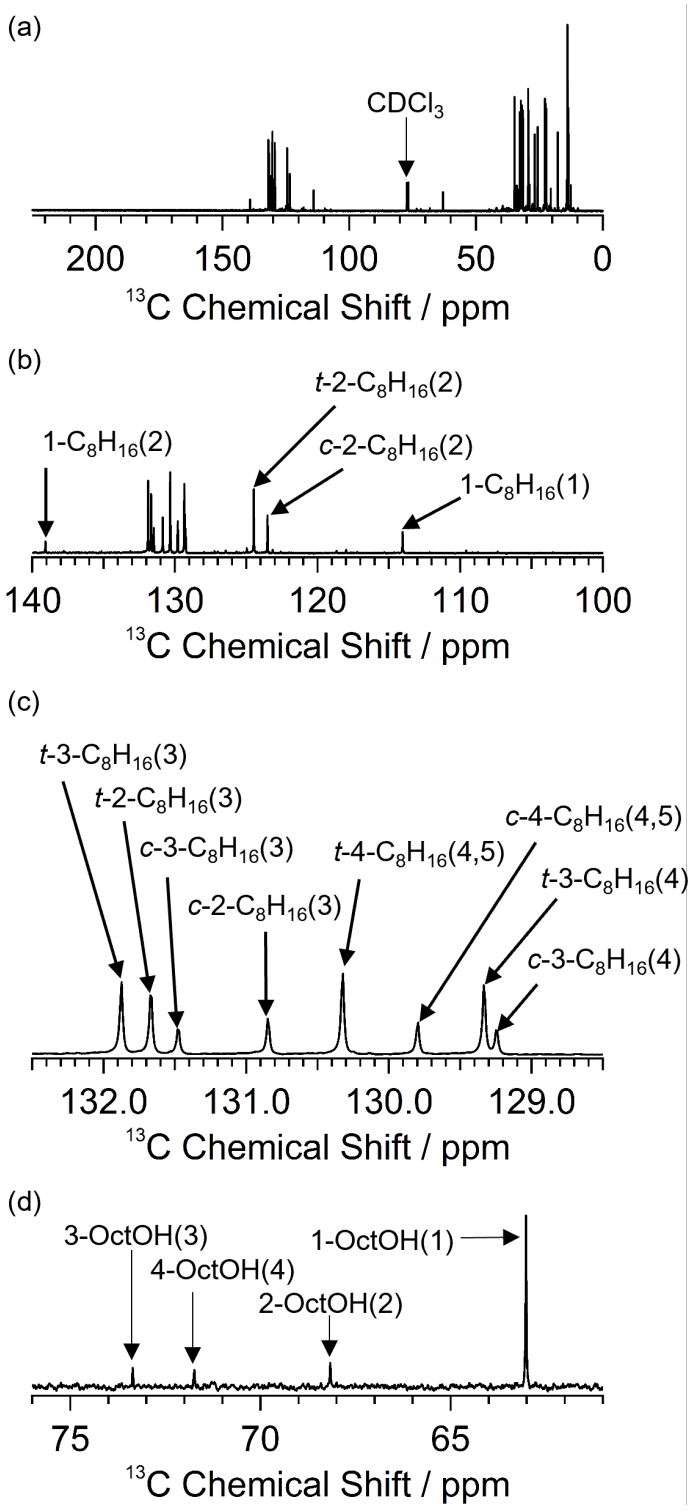
(a)
CDCl3
200
150
100
50
0
13C Chemical Shift / ppm
(b)
t-2-C8H16(2)
1-C8H16(2)
c-2-C8H16(2)
1-C8H16(1)
140
130
120
110
100
13C Chemical Shift / ppm
(c)
t-3-C8H16(3)
t-2-C8H16(3)
c-3-C8H16(3)
t-4-C8H16(4,5)
c-4-C8H16(4,5)
c-2-C8H16(3)
t-3-C8H16(4)
c-3-C8H16(4)
132.0
131.0
130.0
129.0
13C Chemical Shift / ppm
(d)
3-OctOH(3)
4-OctOH(4)
2-OctOH(2)
1-OctOH(1)
75
70
65
13C Chemical Shift / ppm

Figure 9. The ^{13}C NMR spectrum of the products of OctACl in the oil phase dissolved in $CDCl_3$ after the supercritical water reaction at 400 °C for 10 min at 0.20 g cm^{-3}; (a) entire chemical shift region and the enlarged views of (b) the carbon-carbon double-bond region, (c) the 129–132 ppm region where many double bond signals are observed, and (d) the region of octanol signals. The letters *c* and *t* before the name of each octene isomer refer to *cis* and *trans*, respectively. The number in parentheses after the name of each octene isomer indicates the numbering of the carbon atom.

To evaluate the extent to which octene isomerization proceeds, the ratios of the octene isomers were examined. Figure 10 shows the distribution of the isomers of octene in the oil phase produced at 400 °C for 10 min at 0.20 g cm^{-3}. For comparison, Figure 10 also shows the estimated fraction values at equilibrium in the dilute gas phase obtained from the tabulated thermodynamic data.[41] There is overall agreement between the present experimental results and the calculated values, albeit with minor differences. This suggests that the octenes isomerize rapidly, reaching the equilibrium at most in 10 min when the reactant is $OctAH^+$.

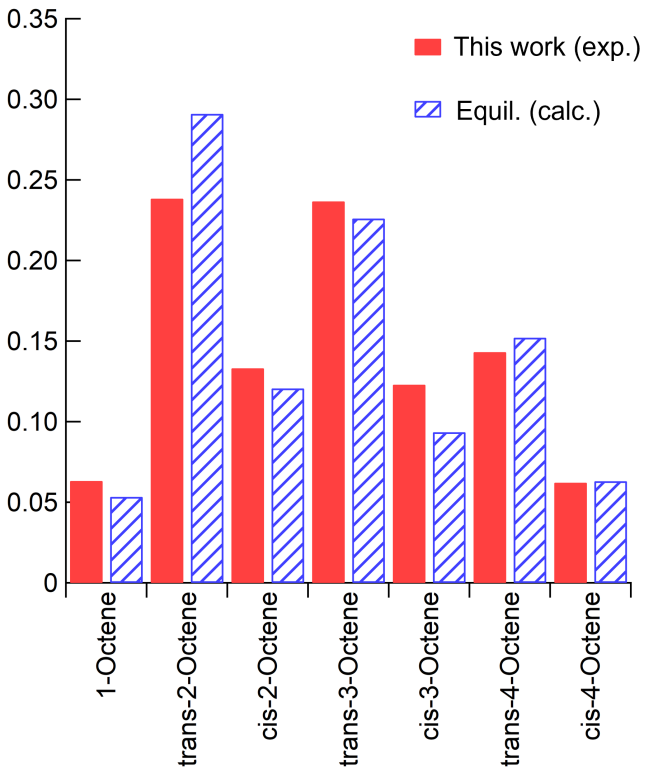

Figure 10. Distribution of octene isomers produced from $OctAH^+$ in the supercritical water reaction. The temperature, the reaction time, and the initial concentration of $OctAH^+$ were 400 °C, 10 min, and 1.0 mol kg^{-1}, respectively. The calculated values at equilibrium are the estimation based on ref. [41].

Let us move on to compare the reaction of neutral OctA and the protonated $OctAH^+$. Figure 11 shows the ^{13}C NMR spectrum of the products of the reaction of OctA and the remaining reactant dissolved in $CDCl_3$; the reaction of OctA was much slower than that of $OctAH^+$ and was conducted for 16 h at 400 °C at 0.20 g cm^{-3} with the initial concentration of 1.0 mol kg^{-1}. The OctA reaction is orders of magnitude slower than that of the corresponding ammonium cation $OctAH^+$. This significant difference due to protonation is well analogous to the difference in the rate between EtA and $EtAH^+$. The reaction time was significantly longer

than that for $OctAH^+$, and 71% of the reactant OctA was remaining. The ^{13}C NMR spectrum in Figure 11 indicates that 1-OctOH and 1-C_8H_{16} are the main products, unlike those from $OctAH^+$. The other octene isomers, 2-, 3-, and 4-C_8H_{16}, could not be detected by ^{13}C NMR because of the production amounts in this reaction condition being below the detection limit, but were detected by the ^1H NMR measurement as overlapping 2-, 3-, and 4-C_8H_{16} signals, as shown in Figure S4. The yields of 1-C_8H_{16} and total 2-, 3-, and 4-C_8H_{16} from the ^1H NMR signal intensities were 2.5% and 0.2%, respectively. The high fraction of 1-C_8H_{16} among octene isomers indicates that octene isomerization is far from the equilibrium ratios shown in Figure 10. Both the slow consumption of OctA and the slow isomerization of octene can be attributed to the fact that those reactions are acid catalyzed; the pH value of 1.0-mol dm^{-3} OctAHCl aqueous solution is 5.3 at room temperature. The yields of 1-OctOH and diOctA are only 2.3% and 2.4%, respectively. In addition to the above, peaks of unknown products with yields of 4%, 12%, and 10% were observed in the oil, aqueous, and vapor phases, respectively. The mass balance of the reactant and the products is 104%.

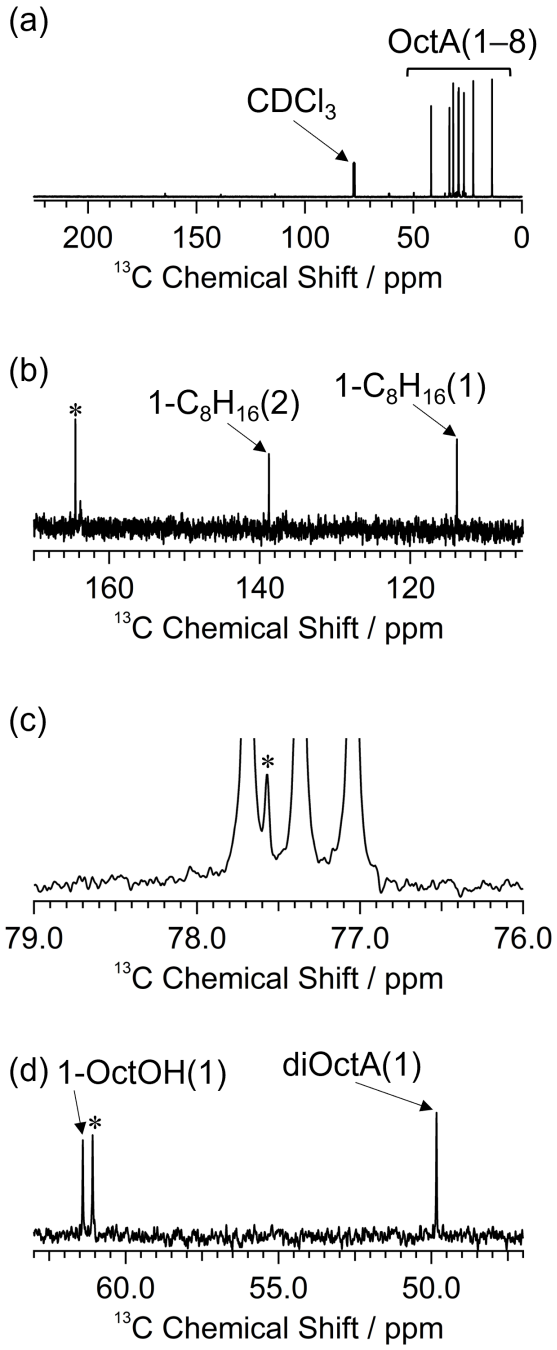

Figure 11. The ^{13}C NMR spectrum of the products of OctA in oil phase dissolved in $CDCl_3$ after the supercritical water reaction at 400 °C for 16 h at 0.20 g cm^{-3}; (a) the entire chemical shift region and the enlarged views of (b) the carbon-carbon double bond region, (c) chloroform signals, and (d) the region of 1-OctOH and diOctA. The signals with asterisks are those of unknown products.

Let us focus on the reaction pathways. The reaction schemes for OctACl and OctA are summarized in Figure 12. In the reaction of OctACl, the ionization equilibrium between $OctAH^+$ and OctA is greatly shifted to the $OctAH^+$ side, making the former the dominant state of the substrate. The initial products from $OctAH^+$ are 1-OctOH and 1-octene (1-C_8H_{16}). The formation of 1-OctOH and 1-C_8H_{16} from $OctAH^+$ constitutes the initial stages of the reactions of $OctAH^+$, and this is also the case for OctA. When OctA is the reactant, the decrease of OctA is much slower than that of $OctAH^+$; the concentration of $OctAH^+$ is low enough to slow the formation of 1-OctOH and 1-C_8H_{16} in neutral or basic conditions. There are two possible mechanisms for the formation of 1-OctOH from $OctAH^+$, the S_N1 and S_N2 pathways: the reaction mechanisms for $OctAH^+$ are in parallel with those for $EtAH^+$ in Figure 8. The formation of 1-OctOH from $OctAH^+$ can also occur via S_N2. The formation of 1-OctOH is assumed to proceed also via the S_N1 mechanism at high temperatures above the critical. Since equilibrium is reached so rapidly under the present experimental conditions, it is difficult to determine whether the S_N1 or S_N2 pathway is more plausible. The mechanism of dehydration of 1-OctOH to 1-C_8H_{16} could either be primarily E2 or E1 is in competition with E2. It is difficult to conclude which of these two possibilities is more likely because the population of protonated 1-OctOH (1-$OctOH_2^+$) cannot be identified. This is analogous to what we have described for the reaction of EtOH to C_2H_4.

Here we consider why the protonated $OctAH^+$ produces a greater variety of olefinic product isomers than the neutral OctA. When $OctAH^+$ is the reactant, 2-OctOH and 2-C_8H_{16} are rapidly produced in addition to 1-OctOH and 1-C_8H_{16}. Once the primary carbocation is formed from 1-OctOH and 1-C_8H_{16}, the rearrangement from the less stable primary carbocation into the more stable secondary carbocation should occur efficiently, leading to the

production of 2-OctOH and 2-C_8H_{16}. Isomerization occurs by dehydration and rehydration. These reactions are acid catalyzed, consistent with the observation that isomerization is faster when the reactant is $OctAH^+$ than when it is OctA.

For the dehydration reaction from 2-OctOH to 2-C_8H_{16}, there are two elimination pathways, the direct E2 pathway and the E1 pathway via a carbocation intermediate, similar to the pathway from 1-OctOH to 1-C_8H_{16}. In the 2-OctOH dehydration, the relative contribution of the E1 pathway is considered to be larger than that in the 1-OctOH dehydration due to the stability of the secondary carbocation intermediate. The formation of 3-OctOH to 3-C_8H_{16} and 4-OctOH to 4-C_8H_{16} can be due to the same scheme. The time scales for the formation of 3-OctOH to 3-C_8H_{16} as well as 4-OctOH to 4-C_8H_{16} are not separable from that for the formation of 2-OctOH to 2-C_8H_{16}, due to the very rapid rearrangements between the carbocation intermediates. Note that 2-C_8H_{16} and 3-C_8H_{16} can also be formed from 3-OctOH and 4-OctOH, respectively, because the protons at both sides of the carbocation can be abstracted to form the carbon-carbon double-bond. Our preliminary examinations with longer reaction times have suggested the formation of various additional products. Elucidation of the subsequent steps is one of the most important issues to be investigated in our future studies. For the OctAHCl reactant, which reacts rather easily, the octene isomer formation step and the subsequent unresolved steps can be more clearly separated. For the OctA reactant, the reaction is much slower and before the conversion to the octene isomer is complete, the subsequent steps become more significant. By focusing on OctAHCl, we have succeeded in detecting the product species summarized in Figure 12 within the reaction time of this study.

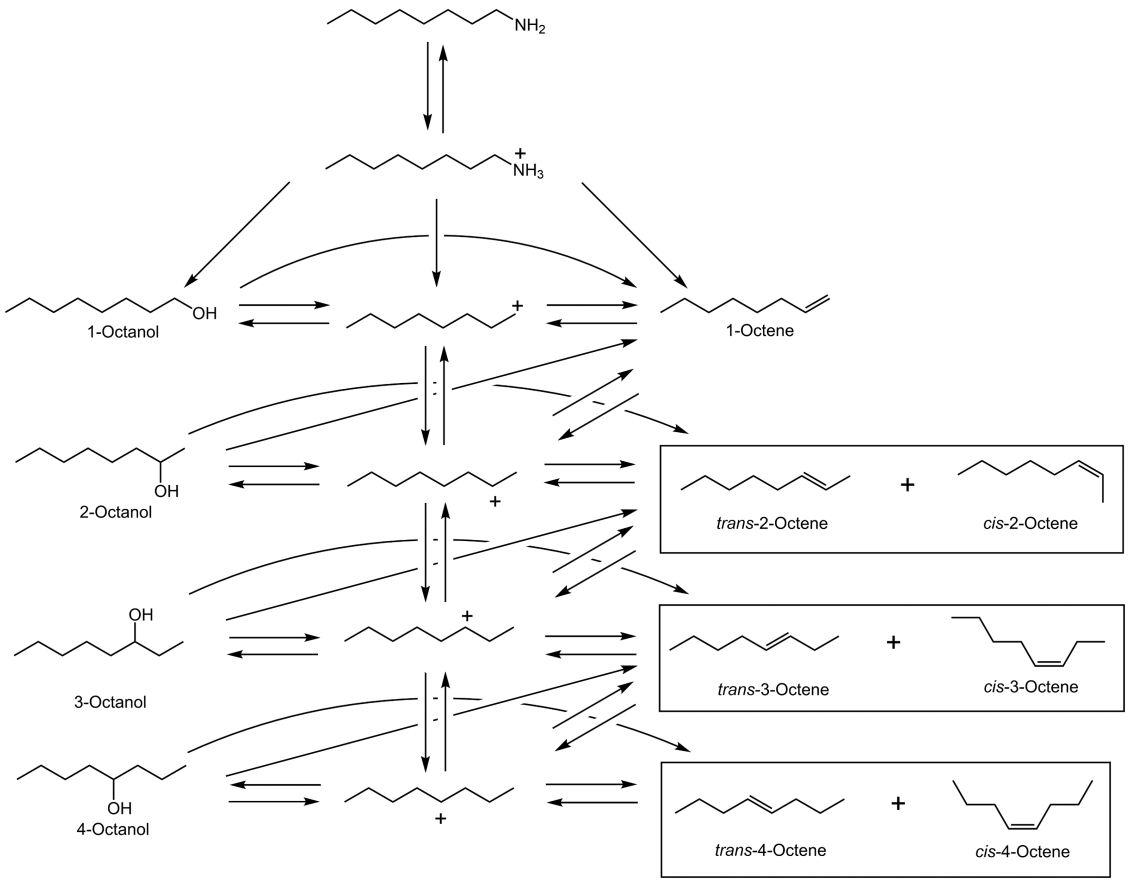

Figure 12. Reaction scheme $OctAH^+$ and OctA in sub- and supercritical water.

It is worthwhile to briefly mention here the often-discussed issue of whether the reaction mechanism in supercritical water is ionic or radical. As discussed above, the reactions studied here can be explained by ionic reaction mechanisms. This is because the reactants and transition states are sufficiently hydrated under the temperature and density conditions studied. Among the thermodynamic conditions under which the hydrothermal reaction was

performed, the reaction products and pathways at the supercritical temperature of 400 °C with 0.2 g cm^{-3} are essentially the same as those at 300 °C (0.71 g cm^{-3}) and 350 °C (0.57 g cm^{-3}) on the liquid-gas coexistence curve. One of the earliest studies of the hydrothermal reactions of amines is the reaction analysis of benzylphenylamine by Abraham and Klein[42] in sub- and supercritical fluids. They showed that the major products in neat and non-polar organic solvent, tetralin, were aniline and toluene, which are products of hydrogenation reactions from some other unspecified hydrogen source. On the other hand, they observed benzyl alcohol, the product of the hydrolysis, as a main product of the reaction in sub and supercritical water, which is markedly different from those in neat and tetralin. Thus, the studies of Abraham and Klein and ours show the generality that hydrolysis of amines is the main pathway in the initial stage of the reaction, regardless of the reactant amine species. At a density of 0.2 g cm^{-3}, water is surrounded by multiple water molecules that form hydrogen bonds, limiting its rotational motion, as found by NMR experiments and computational chemistry studies on supercritical water as a pure solvent;[43-44] rotational motion becomes free rotor-like at about 0.01 g cm^{-3} or less. In previous studies on the supercritical water reaction of aldehydes with carboxylic acids,[23, 45] the reaction was analyzed down to the lowest density of 0.10 g cm^{-3}, and the chemical bond cleavage was found to be heterolytic rather than homolytic. Although there are some minor unassigned byproducts in the present reaction analysis, the major products are limited in variety and can hardly be explained by radical reactions.

Conclusions

The hydrothermal reactions of EtA and OctA as representative alkylamines were analyzed in detail using NMR. Using protonated species $EtAH^+$ cation isotopically labeled with ^{13}C and ^{15}N nuclei, we were able to take advantage of the high sensitivity and scalar coupling to obtain the detailed molecular structure and yield information of the reaction products. In addition to the initial hydrolysis of the primary ammonium $EtAH^+$ to EtOH and NH_4^+, the disproportionation to the secondary ammonium $diEtAH^+$ cation has been found to occur. Dehydration of EtOH to C_2H_4 is also found to take place. $EtAH^+$, EtOH, and $diEtAH^+$ reach equilibrium, and the formation of $triEtAH^+$ is detected after more than 5 hours of reaction time 300 °C. The estimated order of yields of these products at equilibrium is: $EtAH^+ > diEtAH^+ \approx EtOH > triEtAH^+$.

The reactant OctA hydrothermally produce alcohols by the hydrolysis, followed by the subsequent formation of an alkene from the alcohols by dehydration. These reactions are common to EtA. The difference from EtA is that OctA gives complicated products, in which isomerization occurs by shifting the position of the hydroxy group and the double bond. We have successfully determined the structures and amounts of isomers produced, taking advantage of the powerful NMR technique. A comparison of the reaction kinetics and mechanisms of the $OctAH^+$ ion with those of the neutral OctA has highlighted the effects of amine ionization equilibrium and pH. The hydrolysis of the ammonium ion is orders of magnitude faster. It has been proven that the reaction proceeds from the ammonium ion and thus the abundance of ammonium ion due to ionization equilibrium is critical to the rate of degradation of the reactant amine. Isomerizations of both

OctOH and C_8H_{16}, products from OctA and $OctAH^+$, are found to be catalyzed by protons, wherein the intermediates are carbocations.

The findings of this study provide a fundamentally new perspective on the application of FFAs. The lack of sufficient knowledge on the decomposition products under high-temperature conditions in the steam–water cycle has been one of the greatest factors that have deterred new applications of FFA. In a previous study,[7] we have already noted that the initial hydrothermal reaction of the lower alkyl amines EtA and BuA is hydrolysis, with the equivalently produced NH_3 acting as a neutralizer and taking over the role of the decomposed amines. The subsequent reactions have also been clarified by this study. The subsequent products found are isomers of alcohols and alkenes, which do not damage steam power plants; this is encouraging the application of FFAs. The formation of the secondary amines is also not a problem for the water-steam cycle. We assume here that the secondary amines equilibrate with the primary amines in hot water, as in the case with aromatic amines.[32]. By using the ammonium ions that are more reactive than the neutral amines, we have succeeded in obtaining a comprehensive picture of the reaction pathways leading to the formation of various isomers of alcohols and alkenes. In the application of FFA, on the other hand, the pH is maintained between 9 and 10 by adding ammonia or low molecular weight amines for corrosion protection, so the concentration of ammonium ions and protons in the FFA is kept very low. This is advantageous for maintaining the effect of the added FFA for a longer period. The development of practical FFA procedures is strongly supported by the time-consuming basic investigation carried out here. All information on the hydrothermal stability of the amines and products is not only of academic importance but also of practical importance as stated in INTRODUCTION.

Supporting Information.

The Supporting Information is available free of charge at https://pubs.acs.org/doi/10.1021/acs.jpca.3c01213.

Liquid-phase ^{13}C NMR spectra of the aqueous solution of $EtAH^+$ treated for 6 h and 20 h at 300 °C, enlarged view of the ^1H NMR signal of C_2H_4 observed in the liquid-phase as a product of the $EtAH^+$ reaction for 6 h at 300 °C, and enlarged view of the ^1H NMR signal of the product octene isomers in oil phase dissolved in $CDCl_3$ after the supercritical water reaction of OctA at 400 °C for 16 h at 0.20 g cm^{-3} (PDF)

Acknowledgements

This study is supported by Grants-in-Aid for Scientific Research (Nos. 19K05585 and 20K05433) from the Japan Society for the Promotion of Science (JSPS). K.Y. is also grateful for the research fund from the Japan Association for the Properties of Water and Steam (JPAPWS). K.Y. and M.N. greatly appreciate the fruitful discussions with several JPAPWS members interested in FFAs.

References

1. International Association for the Properties of Water and Steam. *Application of Film Forming Substances in Fossil, Combined Cycle, and Biomass Power Plants*, 2019. Technical Guidance Document IAPWS TGD8-16.
2. International Association for the Properties of Water and Steam. *Application of Film Forming Substances in Industrial Steam Generators*, 2019. Technical Guidance Document IAPWS TGD11-19.
3. Betova, I.; Bojinov, M.; Saario, T., Film-Forming Amines in Steam/Water Cycles–Structure, Properties, and Influence on Corrosion and Deposition Processes. *VTT, Espoo, Finland* **2014**.
4. Hater, W., Film Forming Amines – an Appraisal. *PowerPlant Chem.* **2021**, *23*, 162-175.
5. Yoshioka, H.; Yoshida, K.; Noguchi, N.; Ueki, T.; Murai, K.-i.; Watanabe, K.; Nakahara, M., Microscopic Structure and Binding Mechanism of Corrosion-Protective Film of Oleylpropanediamine on Copper in Hot Water. *J. Phys. Chem. C* **2022**, *126*, 6436-6447.
6. Hater, W.; Smith, B.; McCann, P.; de Bache, A., Experience with the Application of a Film Forming Amine in the Connah's Quay Triple Stage Combined Cycle Gas Turbine Power Plant Operating in Cycling Mode. *PowerPlant Chemistry* **2018**, *20*, 136-144.
7. Yoshida, K.; Yoshioka, H.; Ushigusa, N.; Nakahara, M., ^{14}N NMR Evidence for Initial Production of NH_3 Accompanied by Alcohol from the Hydrolysis of Ethylamine and Butylamine in Supercritical Water. *Chem. Lett.* **2021**, *50*, 316-319.
8. Li, J.; Brill, T. B., Spectroscopy of Hydrothermal Reactions, Part 26: Kinetics of Decarboxylation of Aliphatic Amino Acids and Comparison with the Rates of Racemization. *Int. J. Chem. Kinet.* **2003**, *35*, 602-610.
9. Sato, N.; Quitain, A. T.; Kang, K.; Daimon, H.; Fujie, K., Reaction Kinetics of Amino Acid Decomposition in High-Temperature and High-Pressure Water. *Ind. Eng. Chem. Res.* **2004**, *43*, 3217-3222.
10. Klingler, D.; Berg, J.; Vogel, H., Hydrothermal Reactions of Alanine and Glycine in Sub- and Supercritical Water. *J. Supercrit. Fluids* **2007**, *43*, 112-119.
11. Benjamin, K. M.; Savage, P. E., Hydrothermal Reactions of Methylamine. *J. Supercrit. Fluids* **2004**, *31*, 301-311.
12. Li, H.; Oshima, Y., Elementary Reaction Mechanism of Methylamine Oxidation in Supercritical Water. *Ind. Eng. Chem. Res.* **2005**, *44*, 8756-8764.
13. Robinson, K. J.; Gould, I. R.; Hartnett, H. E.; Williams, L. B.; Shock, E. L., Hydrothermal Experiments with Protonated Benzylamines Provide Predictions of Temperature-Dependent Deamination Rates for Geochemical Modeling. *ACS Earth Space Chem.* **2021**, *5*, 1997-2012.
14. Gilbert, R.; Lamarre, C., Thermal Stability of Morpholine Additive in the Steam-Water Cycle of Candu-PHW Nuclear Power Plants. *Can. J. Chem. Eng.* **1989**, *67*, 646-651.
15. Féron, D.; Lambert, I., Thermal Stability of Three Amines in Pressurized Water Reactor Secondary Systems. Laboratory and Loop Experiments. *J. Solution Chem.* **1992**, *21*, 919-932.
16. Domae, M.; Fujiwara, K., Thermal Decomposition of 3-Methoxypropylamine as an Alternative Amine in PWR Secondary Systems. *J. Nucl. Sci. Technol.* **2009**, *46*, 210-215.

17. Kolander, B.; Bache, A. d.; Hater, W., Experience with Treating the Water/Steam Cycle in the Nehlsen Stavenhagen RDF Power Plant with Film-Forming Amines. *PowerPlant Chemistry* **2013**, *15*, 137-145.
18. Sylwestrzak, E.; Moszczynski, W.; Hater, W.; Dembowski, T.; de Bache, A., Experiences with the Treatment of the Water/Steam Cycle of the Adamów Power Plant with Film Forming Amines. *VGB Powertech* **2016**, *8*, 69-74.
19. Xue, Y.; Vughs, D.; Hater, W.; Huiting, H.; Vanoppen, M.; Cornelissen, E.; Verliefde, A.; Brunner, A. M., Liquid Chromatography–High-Resolution Mass Spectrometry-Based Target and Nontarget Screening Methods to Characterize Film-Forming Amine-Treated Steam-Water Systems. *Ind. Eng. Chem. Res.* **2020**, *59*, 22301-22309.
20. Kubo, M.; Takizawa, T.; Wakai, C.; Matubayasi, N.; Nakahara, M., Noncatalytic Kinetic Study on Site-Selective H/D Exchange Reaction of Phenol in Sub- and Supercritical Water. *J. Chem. Phys.* **2004**, *121*, 960-969.
21. Yasaka, Y.; Yoshida, K.; Wakai, C.; Matubayasi, N.; Nakahara, M., Kinetic and Equilibrium Study on Formic Acid Decomposition in Relation to the Water-Gas-Shift Reaction. *J. Phys. Chem. A* **2006**, *110*, 11082-11090.
22. Morris, G. A.; Freeman, R., Selective Excitation in Fourier Transform Nuclear Magnetic Resonance. *J. Magn. Reson.* **1978**, *29*, 433-462.
23. Nagai, Y.; Morooka, S.; Matubayasi, N.; Nakahara, M., Mechanisms and Kinetics of Acetaldehyde Reaction in Supercritical Water: Noncatalytic Disproportionation, Condensation, and Decarbonylation. *J. Phys. Chem. A* **2004**, *108*, 11635-11643.
24. Wagner, W.; Pruß, A., The Iapws Formulation 1995 for the Thermodynamic Properties of Ordinary Water Substance for General and Scientific Use. *J. Phys. Chem. Ref. Data* **2002**, *31*, 387-535.
25. Kang, S.-P.; Lee, J.-W., Hydrate-Phase Equilibria and ^{13}C NMR Studies of Binary (CH_4 + C_2H_4) and (C_2H_6 + C_2H_4) Hydrates. *Ind. Eng. Chem. Res.* **2013**, *52*, 303-308.
26. Park, J.; Kang, S.-P.; Lee, J.-W., ^{13}C NMR Analysis of C_2H_6+C_2H_4+THF Mixed Hydrate for an Application to Separation of C_2H_4 and C_2H_6. *Korean J. Chem. Eng.* **2016**, *33*, 2186-2190.
27. Hesse, M.; Meier, H.; Zeeh, B., *Spectroscopic Methods in Organic Chemistry, 2nd Edition*; Georg Thieme Verlag KG, Stuttgart, 2008.
28. Akitt, J. W.; Mann, B. E., *NMR and Chemistry: An Introduction to Modern NMR Spectroscopy, 4th Ed.*; CRC Press, London, 2017.
29. Yoshida, K.; Matubayasi, N.; Nakahara, M., Self-Diffusion of Supercritical Water in Extremely Low-Density Region. *J. Chem. Phys.* **2006**, *125*, 074307.
30. Peereboom, P. W. E.; Luigjes, H.; Prins, K. O.; Trappeniers, N. J., NMR Spin-Echo Study of Self-Diffusion in Xenon and Ethene. *Physica B+C* **1986**, *139–140*, 134.
31. Suárez-Iglesias, O.; Medina, I.; Sanz, M. d. l. Á.; Pizarro, C.; Bueno, J. L., Self-Diffusion in Molecular Fluids and Noble Gases: Available Data. *J. Chem. Eng. Data* **2015**, *60*, 2757-2817.
32. Robinson, K. J.; Fecteau, K. M.; Gould, I. R.; Hartnett, H. E.; Williams, L. B.; Shock, E. L., Metastable Equilibrium of Substitution Reactions among Oxygen- and Nitrogen-Bearing

Organic Compounds at Hydrothermal Conditions. *Geochim. Cosmochim. Acta* **2020**, *272*, 93-104.
33. The Chemical Society of Japan. ed. *Handbook of Chemistry: Pure Chemistry, 6th Ed.*; Maruzen Publishing Co., Ltd., 2021.
34. Bergström, S.; Olofsson, G., Thermodynamic Quantities for the Solution and Protonation of Four C6-Amines in Water over a Wide Temperature Range. *J. Solution Chem.* **1975**, *4*, 535-554.
35. Robinson, K. J.; Gould, I. R.; Fecteau, K. M.; Hartnett, H. E.; Williams, L. B.; Shock, E. L., Deamination Reaction Mechanisms of Protonated Amines under Hydrothermal Conditions. *Geochim. Cosmochim. Acta* **2019**, *244*, 113-128.
36. Narayan, R.; Antal, M. J., Influence of Pressure on the Acid-Catalyzed Rate Constant for 1-Propanol Dehydration in Supercritical Water. *J. Am. Chem. Soc.* **1990**, *112*, 1927-1931.
37. Xu, X.; De Almeida, C. P.; Antal, M. J., Mechanism and Kinetics of the Acid-Catalyzed Formation of Ethene and Diethyl Ether from Ethanol in Supercritical Water. *Ind. Eng. Chem. Res.* **1991**, *30*, 1478-1485.
38. Bruice, P. Y., *Organic Chemistry, 7th Ed.*; Pearson: New York, 2007.
39. SDBSWeb: https://sdbs.db.aist.go.jp (National Institute of Advanced Industrial Science and Technology, July 1, 2022).
40. Shock, E. L.; Canovas, P.; Yang, Z.; Boyer, G.; Johnson, K.; Robinson, K.; Fecteau, K.; Windman, T.; Cox, A., Thermodynamics of Organic Transformations in Hydrothermal Fluids. *Reviews in Mineralogy and Geochemistry* **2013**, *76*, 311-350.
41. Alberty, R. A.; Gehrig, C. A., Standard Chemical Thermodynamic Properties of Alkane Isomer Groups. *J. Phys. Chem. Ref. Data* **1984**, *13*, 1173-1197.
42. Abraham, M. A.; Klein, M. T., Pyrolysis of Benzylphenylamine Neat and with Tetralin, Methanol, and Water Solvents. *Ind. Eng. Chem. Prod. Res. Dev.* **1985**, *24*, 300-306.
43. Matubayasi, N.; Nakao, N.; Nakahara, M., Structural Study of Supercritical Water. Iii. Rotational Dynamics. *J. Chem. Phys.* **2001**, *114*, 4107-4115.
44. Yoshida, K.; Matubayasi, N.; Nakahara, M., Solvation Shell Dynamics Studied by Molecular Dynamics Simulation in Relation to the Translational and Rotational Dynamics of Supercritical Water and Benzene. *J. Chem. Phys.* **2007**, *127*, 174509.
45. Nagai, Y.; Matubayasi, N.; Nakahara, M., Mechanisms and Kinetics of Noncatalytic Ether Reaction in Supercritical Water. 2. Proton-Transferred Fragmentation of Dimethyl Ether to Formaldehyde in Competition with Hydrolysis. *J. Phys. Chem. A* **2005**, *109*, 3558-3564.

TOC Graphics